



ELSEVIER

Available online at [www.sciencedirect.com](http://www.sciencedirect.com)

SCIENCE @ DIRECT®

Nuclear Instruments and Methods in Physics Research A 513 (2003) 231–238

**NUCLEAR  
INSTRUMENTS  
& METHODS  
IN PHYSICS  
RESEARCH**  
Section A

[www.elsevier.com/locate/nima](http://www.elsevier.com/locate/nima)

# MicroPattern Gas Detectors with pixel read-out

R. Bellazzini\*, G. Spandre

*INFN –Sezioen di Pisa, University the Pisa, Via Livornese 1291, San Piero a Grado , Pisa 56010 Italy*

---

## Abstract

MicroPattern Gas Detectors are position-sensitive proportional counters whose sense electrodes are constructed using microelectronics, thin-film or advanced PCB techniques. The feature size attainable using these methods is of the order of a few microns and the detectors show excellent spatial resolution and fast charge collection. The real challenge with this class of detectors is the design of the read-out system which should not spoil the intrinsic performance of the devices. The most promising approach is the coupling of a pixelized collection anode and read-out system to the gas amplifying stage. We will discuss this principle and we will show examples of practical implementations in the field of X-ray Astronomy and Plasma Imaging.

© 2003 Elsevier B.V. All rights reserved.

*PACS:* 52.70.–m; 52.70.La; 07.85.–m

*Keywords:* MicroPattern; Position-sensitive detector; Pixel read-out

---

## 1. Introduction

The invention of the MicroStrip Gas Chamber has marked a new era in the gas detectors development.

The use of photolithographic techniques has allowed in fact to reach pitches between collecting electrodes of a few hundred microns and thus to obtain very good localization accuracy ( $\sim 30 \mu\text{m}$ ) and very high rate capability (few MHz/mm<sup>2</sup>). Despite their clear advantages with respect to the more traditional gas detectors, the MSGCs are generally fragile devices and still relatively expensive relying on a rather advanced technology. Recently, it has been introduced an innova-

tive class of position sensitive gas detectors that exploits the procedures normally used to built multi-layer printed-circuit boards (PCBs). The Gas Electron Multiplier (GEM) [1], the Micro-Groove [2], the Compteur A Trous (CAT) [3] and the WELL detector [4] are examples of devices based on this technology. A very attractive feature of the GEM consists in the possibility of decoupling the charge-amplifying region from the collecting electrodes. In this way it is possible, by structuring the read-out PCB in a multi-pixel pattern, to get a full 2D capability. The very high granularity of the read-out plane allows also to preserve the intrinsic resolving power and the high rate capability of the device that otherwise would be unavoidably lost by using a conventional projective read-out approach. Applications of a GEM coupled to a pixelized read-out electrode are presented.

---

\*Corresponding author.

*E-mail address:* [ronaldo.bellazzini@pi.infn.it](mailto:ronaldo.bellazzini@pi.infn.it)  
(R. Bellazzini).

## 2. The GEM coupled to a pixelized MicroPattern read-out

The GEM is a thin ( $50\ \mu\text{m}$ ) Kapton foil, metal-clad on both sides and chemically pierced by a regular matrix of holes typically  $60\ \mu\text{m}$  in diameter and  $90\ \mu\text{m}$  pitch (Fig. 1).

Primary electrons released by ionization in the gas, drift from the topside region (Fig. 2) into the GEM holes, where, on application of a voltage gradient, a high dipole field develops and electrons start to multiply in avalanche.

The focusing effect of the electric field provides high transfer efficiency. Electrons passing through the holes into the transfer gap (Fig. 3) are collected by the read-out electrodes that can be freely structured in pixels or pads to get full bi-dimensional reconstruction capability.

The GEM gives also the trigger signal to read-out electronics. Proportional gains above  $10^3$  are obtained in most common gas mixtures. The output signal is proportional to the charge collected by the read-out electrodes and quite fast corresponding to the drift time of the electrons in the transfer gap ( $\sim 20\ \text{ns}$  FWHM in a 2 mm gap).

## 3. X-ray astrophysical polarimetry

In this application the high positional granularity in 2D is exploited to reconstruct photo-electron tracks with just one detection plane.

Polarization of X-ray radiation coming from celestial sources may derive from various processes:

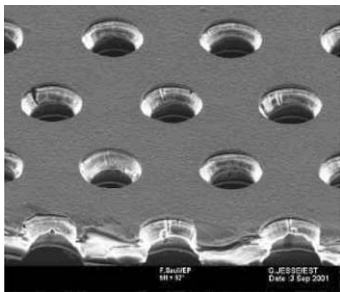


Fig. 1. Microphotograph of a GEM.

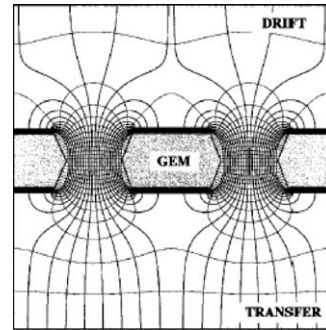


Fig. 2. Field lines in the Gas Electrons Multiplier.

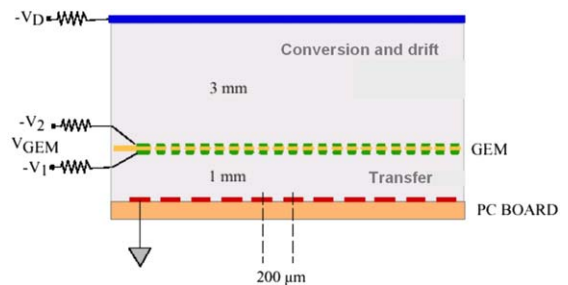


Fig. 3. Schematics of a GEM detector coupled to a MicroPattern read-out.

- emission processes themselves such as cyclotron, synchrotron, non-thermal bremsstrahlung [5];
- scattering on aspherical accreting plasmas: disks, blobs, columns [6];
- vacuum polarization and birefringence through extreme magnetic fields [7,8].

Polarimetric studies of the radiation emitted by Neutron Stars, Galactic and Extragalactic Black Holes and Active Galactic Nuclei are a very attractive item for astrophysicists. At the moment the only accepted measurement of X-ray polarization dates more than 25 years ago. It refers to the observation of the Crab Nebula with a Bragg crystal polarimeter flown on board of the satellite OSO-8 [9]. Unfortunately, conventional polarimetric techniques based on Bragg diffraction at  $45^\circ$  or Compton scattering around  $90^\circ$  are poorly efficient. For this reason a new device based on the

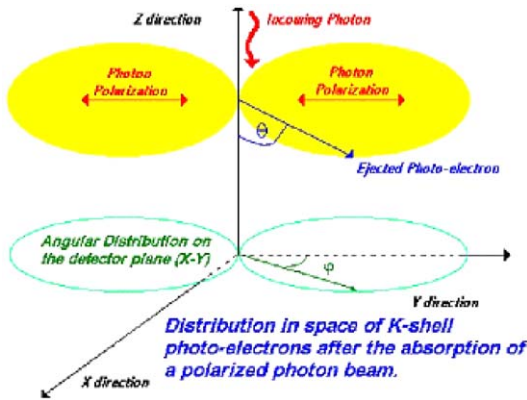


Fig. 4. Angular distribution on the detector plane (XY) of the ejected photoelectrons.

photoelectric effect and highly efficient in the energy range 2–10 keV has been developed.

The photoelectric effect is a process very sensitive to photon polarization and with a large cross-section at low energy. In the case of linearly polarized photons, the differential photoelectron cross-section has a maximum in the plane orthogonal to the direction of the incoming photon and varies with  $\theta$  (the polar angle) and  $\phi$  (the azimuthal angle) as follows (Fig. 4):

$$\frac{d\sigma}{d\Omega} = r_0^2 Z^5 \alpha^4 \left(\frac{m_e c^2}{h\nu}\right)^{7/2} \frac{4\sqrt{2} \sin^2 \theta \cos^2 \phi}{(1 - \beta \cos \theta)^4}. \quad (1)$$

The photoelectron is ejected with maximum probability in the direction of the photon electric field with a  $\cos^2 \phi$  modulation. Fig. 5 shows the principle of operation of the MicroPattern Gas Detector (MPGD), developed to efficiently track the photoelectron [10].

In the above scheme the photoelectron track is projected onto a plane perpendicular to the incoming radiation (Fig. 6). Electrons of the track pass through the GEM where the cascade process takes place. The amplified charge is then collected onto the read-out plane. The photoelectron track, of the order of 1 mm, is well sampled by pixels at 200  $\mu\text{m}$  pitch and reconstructed in two dimensions with very good resolution.

Information on the dynamics of the photoelectron energy loss is also contained in the track

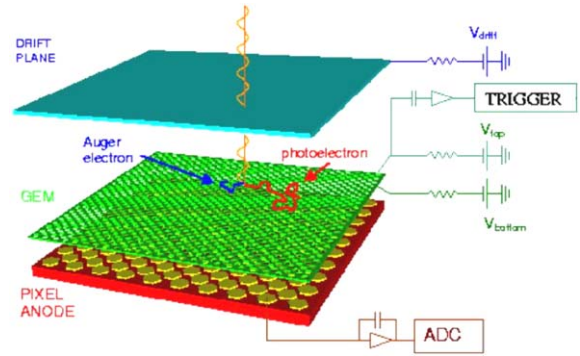


Fig. 5. The MPGD read-out plane is grounded, while both sides of the GEM and the drift plane are at increasingly negative high voltage.

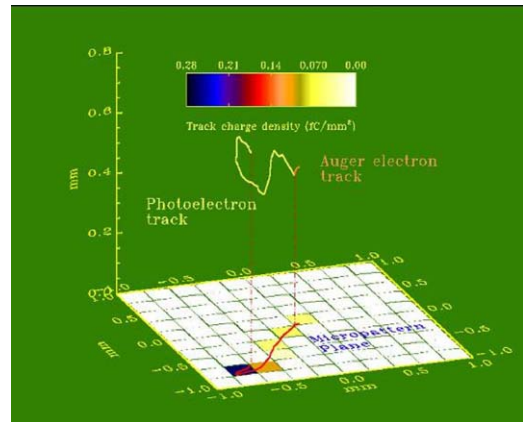


Fig. 6. Polarization information is derived from the track of the photoelectrons imaged by a finely subdivided gas detector.

image. A photo of the multi pixel read-out plane with the connected electronics is shown in Fig. 7.

Drift plane and GEM have been glued with two fibreglass spacers of 6 mm (absorption gap) and 1.5 mm (transfer gap), respectively, over the read-out plane.

The MPGD has been filled with a gas mixture of Neon (80%)—dimethylether (20%) at 1 atm pressure.

The choice of the gas mixture is critical and it is based on a good compromise between high efficiency (increasing with  $Z$ ) and good track reconstruction (conversely decreasing with increasing  $Z$ ).

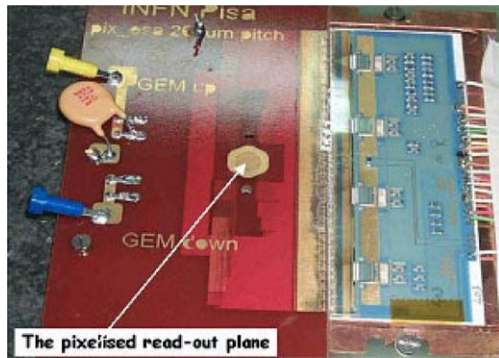


Fig. 7. The multi-pixels read-out plane. Pixels are 512 at 200  $\mu\text{m}$  pitch.

A low  $Z$  gas mixture is preferable due to the high stopping power/scattering ratio and reasonable detection efficiency. Moreover due to the low energy  $K$ -edge of these mixtures, the Auger electrons that are emitted isotropically will get only a small fraction of the photon energy and they will not blur the directional information. Finally, in low  $Z$  gas, tracks are longer so angular reconstruction is easier.

The MPGD has been tested with unpolarized (5.9 keV from a  $^{55}\text{Fe}$  source) and polarized radiation obtained by Thompson scattering on a Li target of photons produced by an X-ray tube. A double diaphragm collimator limited the scattering angles to  $90 \pm 5^\circ$ . In this way the radiation results linearly polarized at 98%.

The direction of emission of the photoelectron is reconstructed by using a two-step algorithm [11,12].

Fig. 8 shows reconstructed photo-electron tracks from 5.9 keV unpolarized X-ray radiation.

The absorption point along the major principal axis of the charge distribution on the pixels is evaluated and then it is defined a new cluster of pixels whose distance from the impact point is less than a set threshold. The new principal axis of this distribution is the reconstructed photoemission direction (Fig. 9).

Fig. 10a shows the angular distribution of the tracks for unpolarized and polarized radiation. As expected, the distribution is flat for the unpolarized case while in the other case it is peaked around the polarization angle and modulated

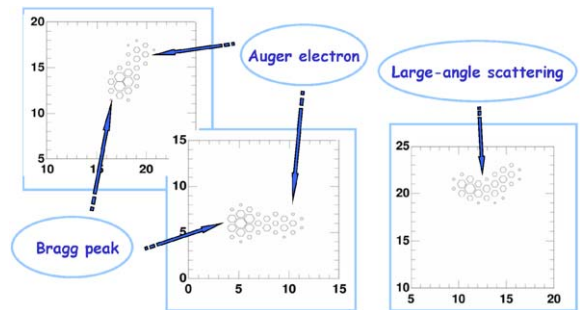


Fig. 8. Sample tracks collected by irradiating the detector with 5.9 keV unpolarized X-rays. Larger boxes correspond to larger energy losses.

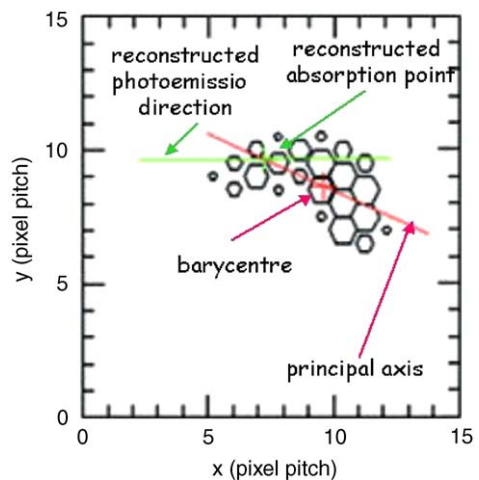


Fig. 9. Real Photoelectron track. Reconstruction of the photoemission direction is done with the identification of the absorption point and the removal of the final part of the track.

according to the function:

$$C(\phi) = A + B \cos^2(\phi - \phi_{\text{pol}}). \quad (2)$$

The constant term is due to the randomization induced by Coulomb scattering while the  $\cos^2$  term derives from the cross-section of the photoelectric effect.

A fundamental parameter in polarimetry is the so-called *modulation factor*. For 100% linearly polarized radiation it results from (2) as follows:

$$\mu = \frac{C_{\text{max}} - C_{\text{min}}}{C_{\text{max}} + C_{\text{min}}} = \frac{B}{2A + B}. \quad (3)$$

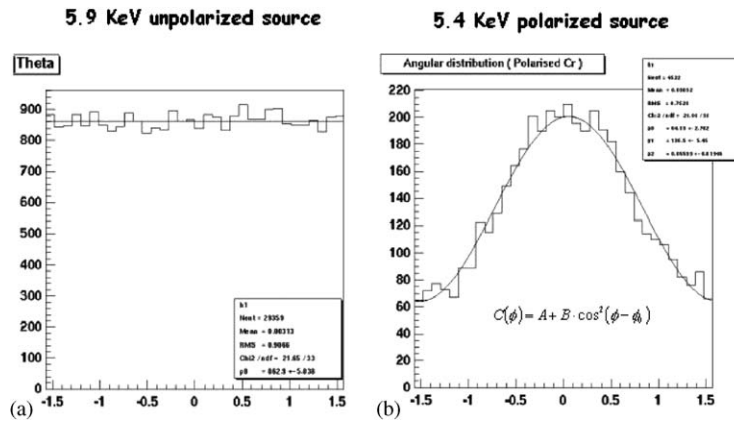


Fig. 10. Cluster angular distribution for unpolarized (a) and polarized radiation (b).

The distribution of Fig. 10b has a modulation factor of  $\sim 50\%$ .

The imaging capability of the MPGD has been also tested. Fig. 11 shows the bi-dimensional plots of barycentres (left) and impact points (right) of the clusters produced in the detector by X-ray radiation passing through a pattern of holes, 500  $\mu\text{m}$  in diameter and 1 mm pitch.

The sensitivity of a polarimeter is usually defined in terms of Minimum Detectable Polarization (MDP) which is the minimum modulated flux needed to exceed, at a defined level of confidence, the statistical fluctuations of both the background and the unmodulated signal (the unpolarized fraction of the source).

At  $n$  standard deviations MPD is

$$\text{MDP}(n_\sigma) = \frac{n_\sigma}{\varepsilon\mu F} \sqrt{\frac{2(B + \varepsilon F)}{ST}}. \quad (4)$$

$F$  is the source flux,  $B$  the background rate,  $S$  the collecting area,  $T$  the observing time and  $\varepsilon$  the detection efficiency. MPD allows evaluating the time necessary to perform a planned measurement.

In the case of negligible background with respect to the source flux (bright sources), which is the case of a polarimeter at the focus of a X-ray optics, the MDP becomes

$$\text{MDP} = \frac{1}{\sqrt{\mu\varepsilon}}. \quad (5)$$

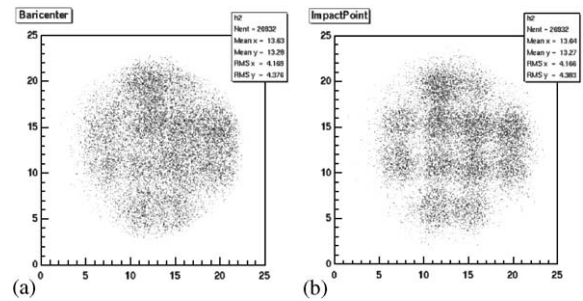


Fig. 11. 2D-image obtained with reconstructed barycentres (left) and impact points (right). In the right plot the pattern of the collimator used is clearly visible.

The tested prototype at the focus of XEUS-1 (the X-ray Evolving Universe Spectroscopy mission) could perform polarimetry at 1% level on many bright AGN in about 1 day observation, in the energy range 2–10 keV.

#### 4. Time-resolved plasma diagnostic

In this second application we have exploited the very high global rate capability offered by the possibility of reading many individual pixels in parallel, each one operating as a free-running individual counter. This new fast system for plasma imaging [13] is based on a pinhole camera coupled to a MPGD with a GEM as amplifying

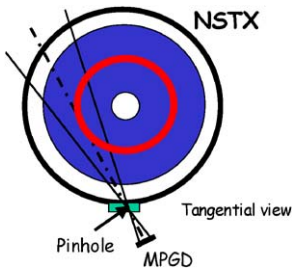


Fig. 12. Sketched view of the NSTX set-up for a tangential view.

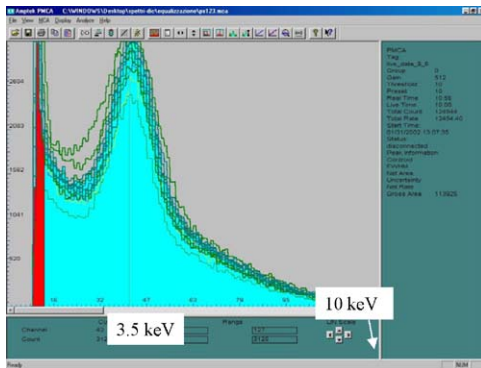


Fig. 13. Spectral response of some pixels to a 1–10 keV source.

stage. The system has been tested on the National Spherical Tokamak Experiment (NSTX) at the Princeton Plasma Physics Laboratory. The device, operating in the soft X-ray energy range, was developed in collaboration between two Italian groups of ENEA (Frascati) and INFN (Pisa).

The detector ( $2.5\text{ cm}^2$ ) is equipped with a 2D read-out PCB with 144 pixels of  $2\text{ mm}^2$  and can take X-ray images of the plasma at very high framing rate (up to 100 kHz), in a selectable energy range and with different magnification or views of the plasma.

A sketch of the set-up with the pinhole camera and the MPGD positioned to get a tangential view of the hottest region of the plasma (1–10 keV) is shown in Fig. 12.

Each pixel has been individually energy calibrated and the gain of each electronic channel finely adjusted in order to reproduce equal spectra of the same source within 2% accuracy (Fig. 13).

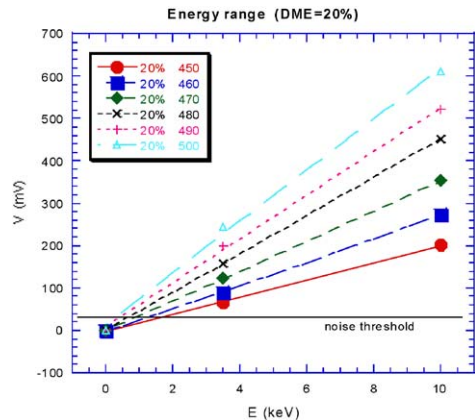


Fig. 14. Energy vs. threshold for various GEM voltages.

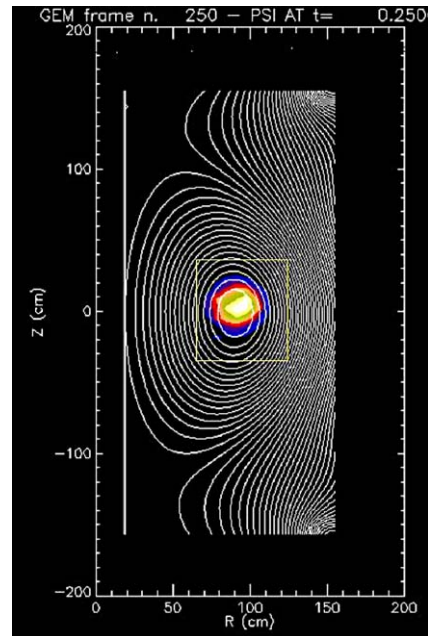


Fig. 15. Centered view of Plasma. The yellow box is  $80 \times 80\text{ cm}^2$ .

Energy discrimination is done by changing either the GEM voltage or the discriminator threshold (Fig. 14). The noise is about  $2000e^-$  (rms) corresponding to a signal of 2 mV.

A 2D centred view of plasma in the energy range 3–8 keV is shown in Fig. 15. The plasma image is  $80\text{ cm}^2$ .

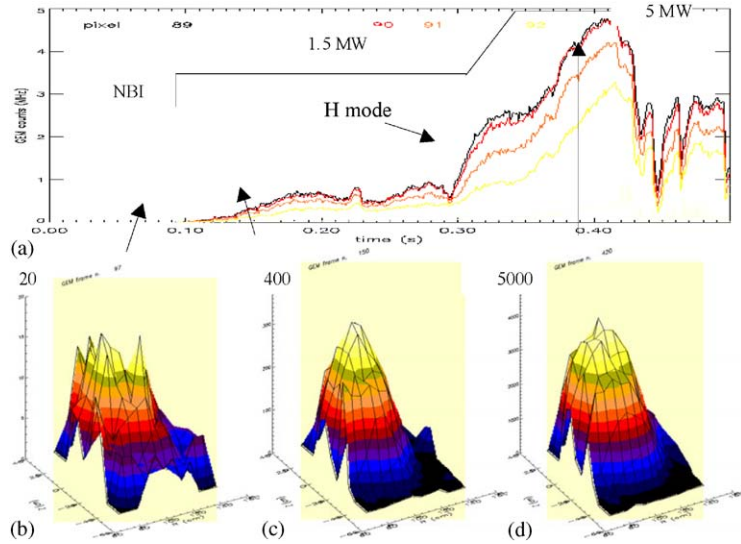


Fig. 16. Time history of some central pixels (framing rate of 1 kHz).

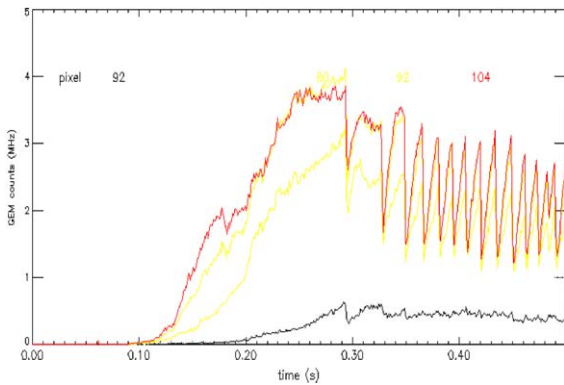


Fig. 17. Time history of some pixels in the central part of the plasma. Strong oscillations are observed in time scale of milliseconds.

The time history of a few central pixels as power is injected into the system, is shown in Fig. 16. The noise of the detector is around 6 counts/pixel and the  $S/N$  at the highest emissivity about 1000. The dynamic range is  $\sim 300$ . Maximum counting rate achieved before saturation is  $10^7$  photons/s · pixel for a global rate of more than  $10^9$  (dead time  $\sim 170$  ns).

Strong oscillations in soft X-ray emission have been observed in the plasma centre (Fig. 17). This effect disappears at  $r \sim 20$  cm.

### 5. Conclusions

Two novel systems for X-ray polarimetry and plasma diagnostic have been checked and validated.

In both cases the MPGD has shown excellent imaging capability. The high granularity ( $\sim 100 \mu\text{m}$ ) of the read-out plane has allowed to efficiently reconstructing photo-electron tracks as short as  $\sim 400\text{--}800 \mu\text{m}$ . Furthermore, the extremely fast acquisition, up to 100 kHz of framing rates, obtained in the second application has allowed following the time evolution of fusion plasmas.

Though the competition with solid state detectors is becoming hard, the field of MPGD is still showing great vitality and propulsion, in particular in applications as X-ray detectors.

Coupling of distributed amplification structures to separate pixel read-out structures seems to be the most exciting perspective.

### References

- [1] F. Sauli, Nucl. Instr. and Meth. A 386 (1997) 531.
- [2] R. Bellazzini, et al., Nucl. Instr. and Meth. A 424 (1999) 444.
- [3] G. Chaplier, et al., Nucl. Instr. and Meth. A 426 (1999) 339.

- [4] R. Bellazzini, et al., *Nucl. Instr. and Meth. A* 423 (1999) 125.
- [5] M.J. Rees, *Mon. Nat. R. Astron. Soc.* 171 (1975) 457.
- [6] R.A. Sunyaev, L.G. Titarchuck, *Astron. Astrophys.* 143 (1985) 374.
- [7] Yu.N. Gnedin, G.G. Pavlov, Yu.A. Shibanov, *Sov. Astron. Lett.* 4 (1978) 117.
- [8] J. Ventura, *Phys. Rev. D.* 19 (1979) 1684.
- [9] M.C. Weisskopf, G.G. Cohen, K.S. Long, H.L. Kenstenbaum, R. Novick, R.S. Wolff, *Astrophys. J.* 208 (1976) L125.
- [10] E. Costa, P. Soffitta, R. Bellazzini, A. Brez, N. Lumb, G. Spandre, *Nature* 411 (2001) 662.
- [11] P. Soffitta, E. Costa, G. di Persio, E. Morelli, A. Rubini, R. Bellazzini, A. Brez, R. Raffo, G. Spandre, D. Joy, *Nucl. Instr. and Meth. A* 469 (2001) 164.
- [12] R. Bellazzini, L. Baldini, A. Brez, E. Costa, L. Latronico, N. Omodei, P. Soffitta, G. Spandre, *Anovel gaseous X-ray polarimeter: data analysis and simulation*, Proceedings of the Conference on Astronomical Telescope and Instrumentation, Waikoloa, 2002.
- [13] D. Pacella, R. Bellazzini, M. Finkhental, A. Brez, G. Pizzicaroli, *AX-VUV imaging system for fusion plasmas based on a Micro Pattern Gas Detector*, *Nucl. Instr. and Meth. A* 510 (2003) Nos. 1–2 (Proceedings of the SAMBA Conference, Trieste 2002).